

Giant Apparent Optical Circular Dichroism in Thin Films of Bismuth-Based Hybrid Organic–Inorganic Metal Halide Semiconductor Through Preferred Orientation

Liang Yan,* Yi Xie, David B. Mitzi, Peter C. Sercel, Alan J. Phillips, Jeffrey L. Blackburn, and Wei You*

Introducing chirality into organic/inorganic hybrid materials can impart chiroptical properties such as circular dichroism. The ability to tune chiroptical properties in self-assembled materials can have important implications for spintronic and optoelectronic applications. Here, a chiral organic cation, (*R/S*)-4-methoxy- α -methylbenzylammonium, is incorporated to synthesize the bismuth-based hybrid organic–inorganic metal halide semiconductor, (*R/S*-MeOMePMA)BiI₄. Thin films of this Bi-based compound demonstrate large chiroptical responses, with circular dichroism anisotropy (g_{CD}) values up to ≈ 0.1 , close to the highest value observed in another chiral metal-halide semiconductor, (*R*-MBA₂CuCl₄). Detailed investigation reveals that this large g_{CD} in (*R/S*-MeOMePMA)BiI₄ is caused by the apparent CD effect. Careful selection of deposition conditions and the concomitant thin-film orientation enables the control of g_{CD} , with maximum value observed when its thin film has a well-crystallized preferred (001) orientation parallel to the substrate. The results support a growing body of evidence that low symmetry plays an important role in achieving unusually large g_{CD} in these chiral metal–halide materials and provides design rules for achieving large chiroptical response via morphology control.

are perhaps the organic/inorganic hybrid perovskites (OIHPs), which have been widely studied for optoelectronic applications such as light emitting diodes, solar cells, and transistors,^[2–5] and the metal–organic chalcogenides, which exhibit in-plane anisotropy and large exciton binding energy.^[6–8] Introducing chiral organic molecules into OIHPs to combine chirality with features rooted in the inorganic sublattice, such as strong absorption, spin-orbit coupling, and quantum confinement (in low-dimensional OIHPs), can lead to intriguing properties^[9–12]—for example, circular dichroism (CD),^[13–15] circularly polarized luminescence (CPL),^[16–18] nonlinear optical properties,^[19–22] chiral-induced spin selectivity effects^[23–25] and chiral-phonon-activated spin Seebeck effect.^[26] Among those, CD is perhaps the most fundamental chiroptical property that describes the difference in the material interaction between left- and right-handed circularly polarized light. The anisotropy

factor (g_{CD}), defined by Equation (1),^[27,28] is commonly used to compare the chiroptical activities between materials:

$$g_{CD} = \frac{\Delta A}{Absorbance} = \frac{CD [mdeg]}{32980 \times Absorbance} \quad (1)$$

1. Introduction

Organic–inorganic hybrid semiconductors (OIHS) are an important family of materials with unique electronic and optical properties.^[1] The most prominent examples in recent years

L. Yan, W. You
Department of Chemistry
University of North Carolina at Chapel Hill
Chapel Hill, NC 27599, USA
E-mail: lyan1@live.unc.edu; wyou@unc.edu

Y. Xie
University program in Materials Science and Engineering
Duke University
Durham, North Carolina 27708, USA

Y. Xie, D. B. Mitzi
Department of Mechanical Engineering and Materials Science
Duke University
Durham, NC 27708, USA

D. B. Mitzi
Department of Chemistry
Duke University
Durham, NC 27708, USA

P. C. Sercel
Center for Hybrid Organic Inorganic Semiconductors for Energy
Golden, CO 80401, USA

A. J. Phillips, J. L. Blackburn
Materials, Chemistry, and Computation Science Directorate
National Renewable Energy Laboratory
Golden, CO 80401, USA

A. J. Phillips
Department of Physics
Colorado School of Mines
Golden, CO 80401, USA

The ORCID identification number(s) for the author(s) of this article can be found under <https://doi.org/10.1002/adom.202302766>

DOI: 10.1002/adom.202302766

where ΔA is the difference of absorbance of the left-handed and right-handed circular polarized light, and CD is the measured circular dichroism signal. Recently, lead-free OIHS, such as bismuth-based^[29,30] or copper-based^[31] OIHS have been developed. Typically, the g_{CD} values for chiral OIHS are in the range of 10^{-4} – 10^{-2} ,^[32] however, a few recent works have reported g_{CD} values of such hybrids to be as high as 0.1 in 0D chiral methylbenzylammonium copper chlorides (*R*-MBA₂CuCl₄),^[31] and 0.04 in 1D naphthylethylammonium lead iodide (*R/S*-NEAPbI₃).^[27]

Such unusually large g_{CD} values have been observed in organic thin films,^[33] but are often accompanied by an inversion of the CD spectrum upon flipping the samples.^[34–37] This peculiar behavior has been attributed to the “apparent CD” effect, which results from the optical interference of the material’s (typically in a thin film) linear dichroism (LD) and linear birefringence (LB) (also referred to as the “LDLB effect”).^[33,37–41] Since the apparent CD effect is linked to the propagating direction of circularly polarized light within the material, reversing the propagation direction inverts the chiroptical response (i.e., inverts the CD spectrum)—a characteristic which has been described as “non-reciprocal” or antisymmetric with respect to the light propagation direction.^[40]

Taking the apparent CD into account, the observed CD signal (CD_{obv}) can be approximated as the sum of genuine CD ($CD_{genuine}$) and the LDLB term as in Equation (2)

$$CD_{obv} \approx CD_{genuine} + \frac{1}{2} (LD' \cdot LB - LD \cdot LB') \quad (2)$$

where LD and LB are the linear dichroism and linear birefringence of the thin film between two orthogonal axes (e.g., x and y) in the plane perpendicular to the propagation direction of the light (the z -axis in this example).^[39,40] LD' and LB' are the linear dichroism and linear birefringence of the thin film measured between two orthogonal axes rotated by 45° about the optical axis. When the thin film is flipped (by rotating the sample 180° about the x -axis in this example), the sign of LD or LB remains the same whereas the sign of LD' and LB' is reversed, resulting in an inverted LDLB term (second term in Equation (2)). Therefore, the genuine CD response ($CD_{genuine}$, first term in Equation (2)) can be extracted by averaging the CD signal measured from two directions (e.g., front and back) of the sample. This method has been recently demonstrated by Lu and co-workers^[38] in determining the apparent CD effect in 1D organic/inorganic hybrid perovskites and 0D chiral metal–halide semiconductors. It is worth noting that “apparent CD” is still a true circular polarized light-matter interaction, which could be utilized in a similar fashion to the genuine CD in applications such as circular polarized light detection^[27,42] (as demonstrated recently by Blackburn’s and Lu’s groups^[31,38]) and emission.^[18,43] It is also worth noting that Ugras et al.^[44] have recently shown that Equation (2) also contains higher-order terms that do not cancel out upon flipping the sample.

Herein, we report a bismuth (Bi)-based 0D organic/inorganic metal halide hybrid incorporating a chiral cation, (*R/S*-MeOMePMA)BiI₄, showing a large chiroptical response (g_{CD}) up to ≈ 0.1 , close to the value obtained with 0D chiral methylbenzylammonium copper chlorides (i.e., (*R*-MBA)₂CuCl₄).^[31] We demonstrate that i) this large g_{CD} is caused by the apparent CD effect and ii) the apparent CD effect exhibits strong orientation

and morphology dependence, with a much larger g_{CD} observed when the thin film has the preferred (001) orientation parallel to the substrate. This strong orientation dependence provides a means by which the deposition conditions of a self-assembled organic/inorganic hybrid system provide sensitive control over the resulting chiroptical response. Our results demonstrate that self-assembled organic–inorganic hybrids are an excellent platform for exploiting the apparent CD effect, which has a lot of potential for circularly polarized light-based devices and applications.

2. Results and Discussion

Methylbenzylammonium is a widely utilized chiral cation in chiral OIHS.^[14,31] In principle, CD has a strong correlation with the exciton transition dipole moment.^[45,46] With this understanding, we chose the modified methylbenzylammonium by introducing a para-substituted polar methoxy group on its benzene ring, resulting in the MeOMePMA. The polar methoxy group in MeOMePMA was proposed to disturb the transition dipole moment in OIHS and impact the CD and anisotropy factor in OIHS. Additionally, the polar methoxy group in MeOMePMA is likely to introduce strong intermolecular interactions, such as hydrogen bonding, between the chiral cations. This could further affect the packing arrangement of these cations around the inorganic clusters, potentially leading to altered CD and anisotropy factor in the resulting OIHS. Therefore, MeOMePMA was selected for the synthesis of a new type of OIHS.

The structure of (*S*-MeOMePMA)BiI₄ was determined from single crystal XRD at room temperature (299 K), as shown in **Figure 1a**. The structure belongs to the *P1* space group, and the details of crystallographic parameters are shown in Table S1 (Supporting Information). We also investigated the crystal structure at 80 K (Table S1, Supporting Information) and found that there is no structural phase transition from 299 to 80 K. The single crystal structure indicates that the material has a 0D structure, comprised of inorganic clusters (four edge-shared octahedra in one unit cell) spaced apart by the chiral organic cations. The views of a $2 \times 2 \times 2$ unit along a , b and c axes are shown in **Figure S1** (Supporting Information). There are nominally six hydrogen bonds (red dot lines in **Figure 1a**) between inorganic clusters and organic cations in one unit cell to stabilize the organic/inorganic hybrid structure at 299K. And as expected there are also hydrogen bonds between organic cations, forming a dimer-like structure, as shown in **Figure 1b**. The details of hydrogen bond geometry in (*S*-MeOMePMA)BiI₄ at 299 K are listed in Table S2 (Supporting Information).

The simulated powder XRD pattern is consistent with the experimental XRD pattern of the powder sample made from single crystals (**Figure 2a**). However, the XRD pattern from the thin film of (*S*-MeOMePMA)BiI₄, cast from the dimethylformamide (DMF):dimethylsulfoxide (DMSO) = 4:1 (by volume) solution, is dominated by a series of (00 l) peaks, indicating a preferred orientation of the (*S*-MeOMePMA)BiI₄ thin film parallel to the substrate plane.

R[representative films of both (*R*- and *S*-MeOMePMA)BiI₄ have almost identical absorption spectra (**Figure 2b**), with an absorption peak at ≈ 530 nm, which was assumed to be from an excitonic state due to the spatial confinement from the inorganic

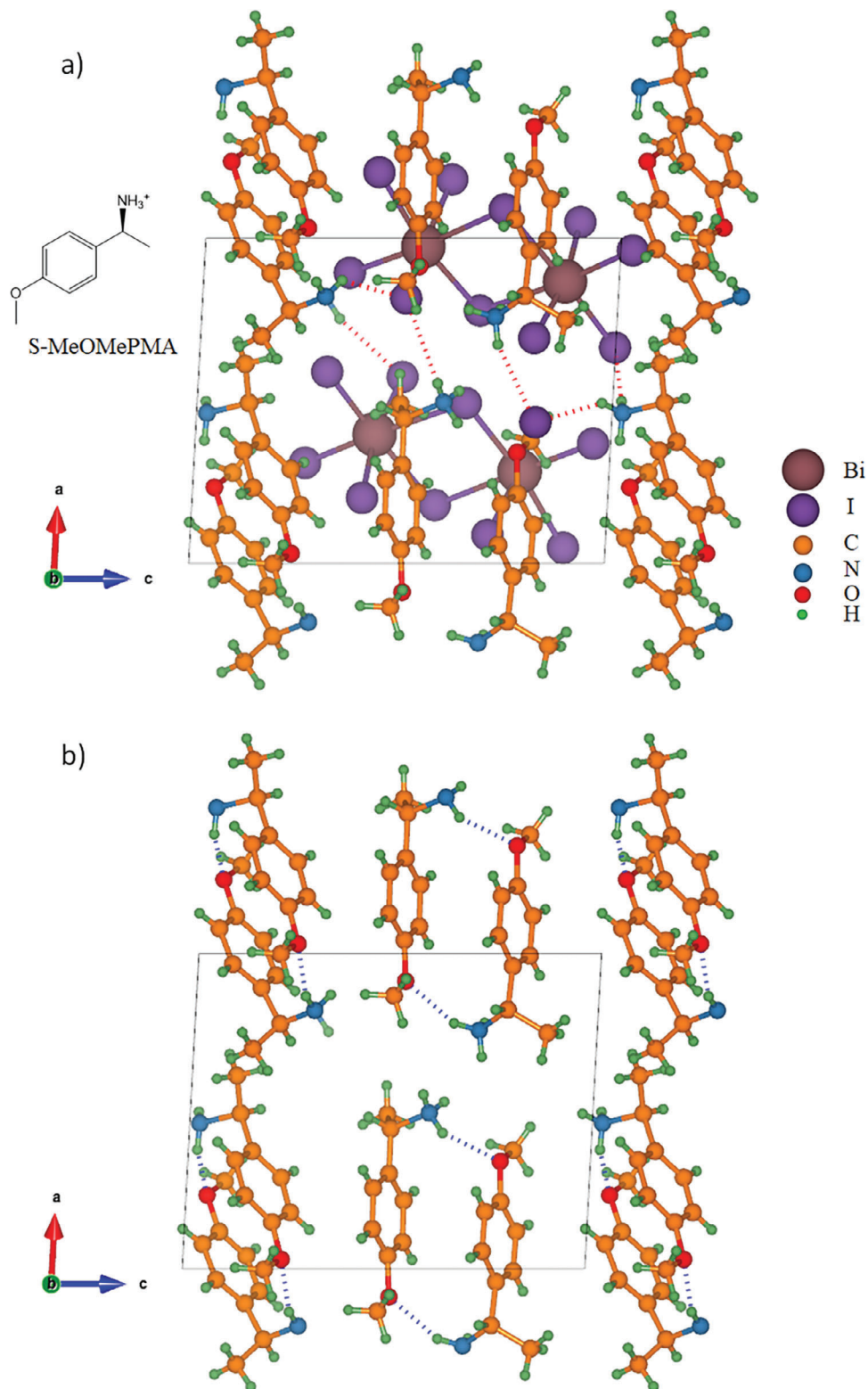


Figure 1. a) Crystal structure of (S-MeOMePMA)Bi₄ at room temperature (view along *b* axis) and chemical structure of S-MeOMePMA, with the red dot lines representing the NH...I hydrogen bonds between organic cations and inorganic clusters, b) the blue dot lines represent the NH...O hydrogen bonds between organic cations, with inorganic clusters being omitted for clarity.

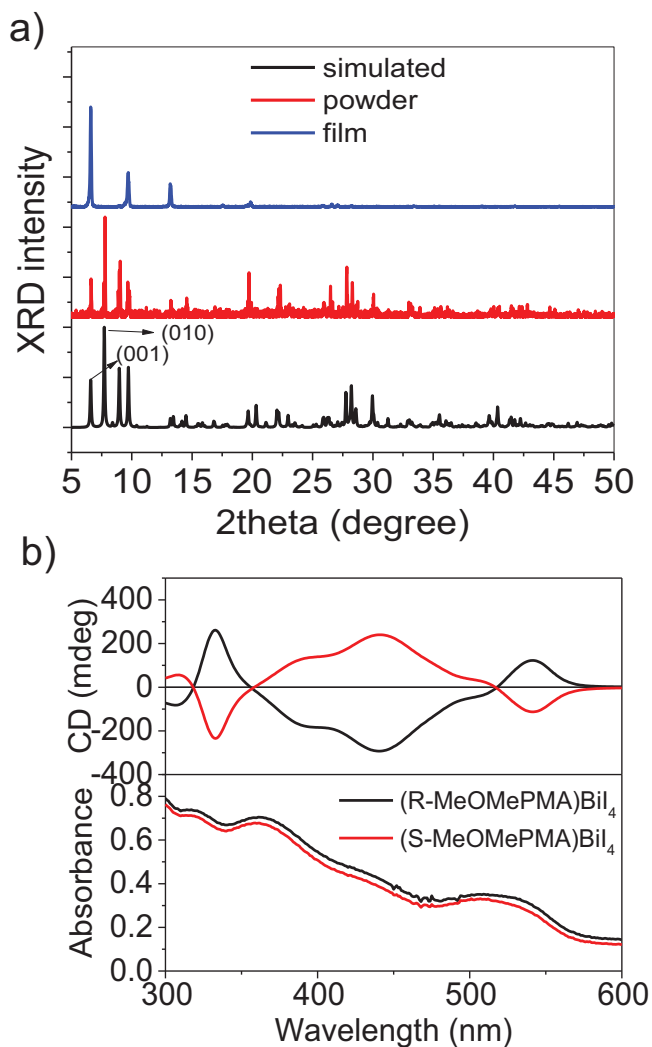


Figure 2. a) XRD patterns of powder (red), thin film (blue) of (S-MeOMePMA)BiI₄ and the simulated XRD pattern (black) from single crystal structure of (S-MeOMePMA)BiI₄, b) absorption and CD spectra of thin films of (R/S-MeOMePMA)BiI₄.

clusters and the dielectric confinement from the surrounding organic cations.^[47] In contrast, the CD spectra are mirror images of each other and the anisotropy factor (g_{CD}) for these films, calculated by Equation (1), is ≈ 0.02 at ≈ 440 nm. To rule out possible effects coming solely from the chiral organic cations, we measured CD and absorption of the organic cation iodide salts, R/S MeOMePMAI, in aqueous solution (Figure S2, Supporting Information), which only showed absorption and CD signals in the range of 200–300 nm and g_{CD} on the order of 10^{-5} . Clearly, the observed chiroptical properties emerge from the inorganic framework of the hybrid organic–inorganic metal halide compound.

The anisotropy factor (g_{CD}) can be largely affected by the thin film morphology, such as the crystallinity and preferred orientation.^[27] To discern the impact of thin film morphology on CD, we varied the annealing temperature from 60 °C to 85 °C for the film of (S-MeOMePMA)BiI₄ casted from the mixed solvent of DMF:DMSO = 4:1, and compared all XRD patterns in Figure 3a.

From 60 to 70 °C, somewhat broad (001) and (010) peaks are clearly observed and the (010) peak is strongest. Samples annealed in this temperature range, with no strongly preferred crystal orientation, exhibit small g_{CD} (Figure 3b). However, from 75 to 85 °C, the (001) peak increases in intensity and the (010) peak almost disappears, indicating better film crystallinity and a strongly preferred (001) orientation parallel to the substrate. This change is accompanied by a substantial change of g_{CD} (Figure 3b; the raw CD signal and absorption spectrum are presented in Figure S3, Supporting Information). For example, a weak (001) peak correlates with a small g_{CD} (less than 0.01), whereas a much stronger g_{CD} (0.02–0.03) is associated with an intensified (001) peak.

These trends indicate that the anisotropy factor (g_{CD}) of the Bi-based organic–inorganic hybrid thin film has a strong (positive) correlation with the diffraction intensity of the (001) peak (Figure 3c). When the $I_{(001)}/I_{(010)}$ is very small the g_{CD} is also small. To probe the additional potential impact of grain size on g_{CD} , we plot the normalized XRD patterns of films annealed at different temperatures in Figure S4 (Supporting Information). The (010) FWHM (full width at half maximum) in films annealed at 60–70 °C (with clear (010) peak and weak (001) peak) were slightly larger than the (001) FWHM in films annealed at 75–85 °C (no (010) peak and strong (001) peak), indicating grain sizes in films annealed at 75–85 °C are just slightly larger than in films annealed at 60–70 °C. Taken together the XRD trends indicate that the crystal quality (i.e., grain size) and the degree of preferred (001) orientation parallel to the substrate may both play important roles in achieving large anisotropy factor (g_{CD}).

Further optimization of the deposition conditions enabled us to significantly enhance the CD response of the films. The film formation of lead halide perovskites and similar metal halide complexes is significantly influenced by the solvents. Solvents have different polarities, viscosities, boiling points, and coordinating ability, and these properties can cause significant differences in solvent evaporation and intermediate formation, which in turn directly affect the crystallization kinetics.^[48] The primary solvent impact is the Lewis acid–base interactions.^[49,50] Considering that BiI₃ acts as a Lewis acid,^[51] solvents with varying dielectric constant or donor numbers exhibit different coordination strengths with BiI₃, leading to different crystallization kinetics. Processing temperature is also known to play a pivotal role in nucleation and growth processes in lead halide perovskites films.^[48] Preheating the substrate to reduce nucleation sites is an effective strategy to ensure controlled crystallization, which initiates gradually from the gas–liquid interface.^[52] Moreover, the surface energy, which influences preferential crystallization at gas–liquid interface, can also vary with changes of the preheating temperature. Therefore, we employ solvent engineering and careful adjustment of preheating temperatures to precisely control the morphology of the (S-MeOMePMA)BiI₄ films, thereby optimizing their chiroptical properties.

By preheating the substrate and using acetonitrile (MeCN):DMSO = 9:1 as the solvent for processing, we achieved g_{CD} values as high as ≈ 0.1 when measured from the front side of the sample (Figure 4a). As shown in Figure S5 (Supporting Information), the XRD pattern of the film cast from MeCN:DMSO showed very strong (001) peak and negligible (010) peak, which gives the $I_{(001)}/I_{(010)}$ of ≈ 56 . However, the g_{CD} obtained from the measurement from the back side was

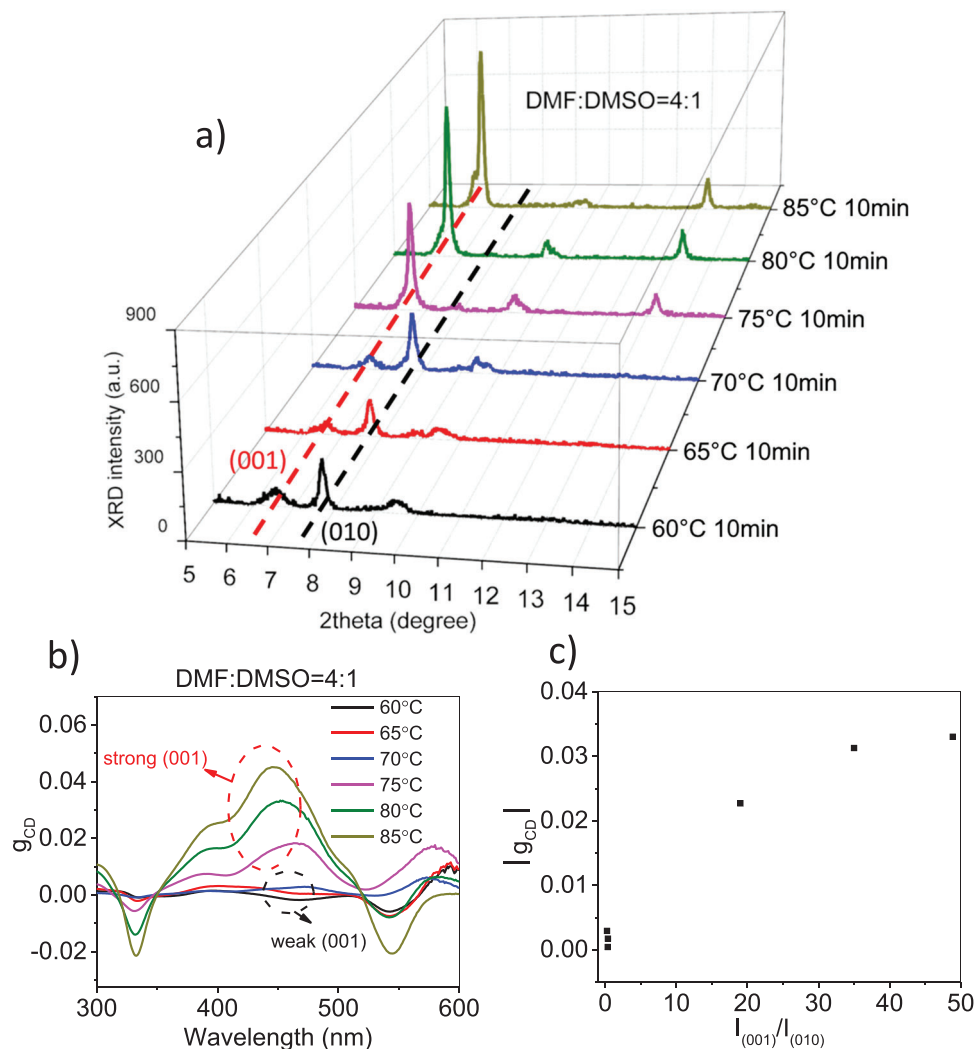


Figure 3. a) XRD patterns of (S-MeOMePMA)BiI₄ films processed from DMF:DMSO = 4:1 at different annealing temperature, b) g_{CD} of (S-MeOMePMA)BiI₄ films annealed at different temperature, c) absolute value of g_{CD} at the peak ≈ 450 nm versus $I_{(001)}/I_{(010)}$, where $I_{(001)}$ and $I_{(010)}$ are the intensities of the (001) peak and (010) peak in the XRD patterns, correspondingly.

inverted, indicating that the unaveraged g_{CD} has a strong contribution from the “apparent CD” effect.^[38,40] When averaging g_{CD} of two measurements (front and back) to extract the genuine CD response and calculating the half of the difference of the front and back measurements to extract the LDLB effect, the $g_{CD(genuine)}$ is more than one order of magnitude smaller and the LDLB effect contributes to most of the unaveraged g_{CD} (Figure 4a; the raw CD and absorption spectra are in Figure S6, Supporting Information). These results are similar to what was recently observed in the 0D chiral metal-halide semiconductor, (R-MBA)₂CuCl₄.^[31,38] To fully appreciate the g_{CD} , one needs to evaluate the entire spectrum, though we typically focus on the g_{CD} from the hybrid material rather than the organic cations. For example, in (R-MBA)₂CuCl₄ film, a value of g_{CD} (≈ 0.1) was achieved at the exciton peak position (≈ 400 nm), yet at the absorption band of R-MBA (270 nm) in (R-MBA)₂CuCl₄, an even larger g_{CD} was observed. Furthermore, no clear g_{CD} was shown for the absorption from Cu d-d transition (600–1400 nm).^[31] In

our case, the maximum of g_{CD} in the (S-MeOMePMA)BiI₄ film was not achieved at the exciton peak position (≈ 530 nm) but at ≈ 450 nm, which should be from another higher energy absorption band of the (S-MeOMePMA)BiI₄ film. Nevertheless, in both (S-MeOMePMA)BiI₄ and (R-MBA)₂CuCl₄ films, absorption bands with large g_{CD} have contributions from LDLB effect.^[38]

Since bismuth (Bi) is the heaviest among all heavy metals and could lead to stronger spin-orbital coupling, the observation of large apparent CD from both triclinic (R/S-MeOMePMA)BiI₄ and monoclinic (R-MBA)₂CuCl₄ suggests that the “heavy element” effect does not play a dominant role in affecting the CD spectrum. Rather, it is likely that the low symmetry of these hybrid organic-inorganic metal halide semiconductors leads to the strong apparent CD effect. Salij et al.^[40] developed a microscopic model for apparent CD based on a Lorentz oscillator model. Their model showed that apparent CD can only occur in systems with non-degenerate electronic transitions whose transition dipoles are neither orthogonal nor parallel. In the context of excitonic

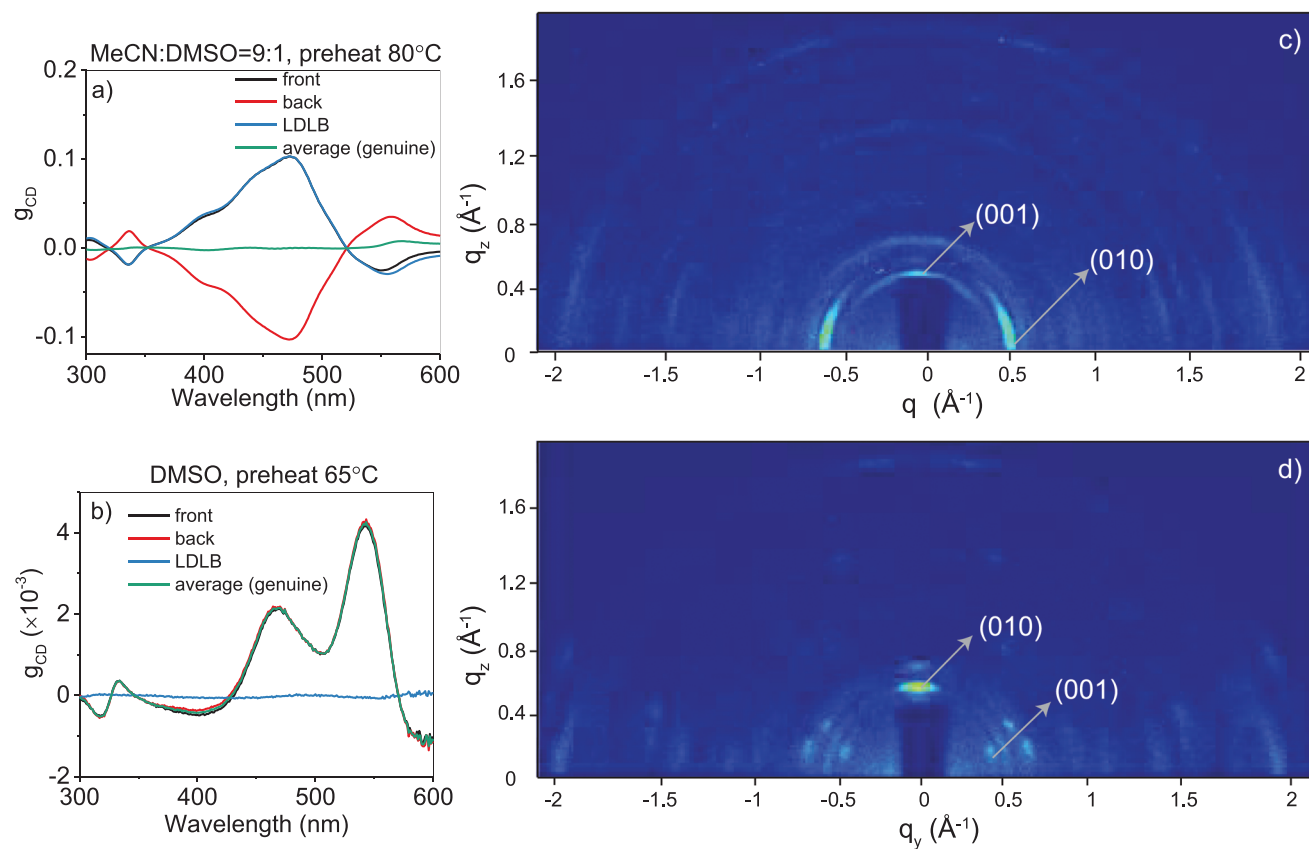


Figure 4. g_{CD} measured from different sides of the (S-MeOMePMA)BiI₄ film by flipping the sample: a) coated from MeCN:DMSO = 9:1 and b) coated from DMSO. Both LDLB effect and averaged (genuine) g_{CD} are shown. (The comparison of averaged (genuine) g_{CD} of (001) and (010) oriented films was shown in Figure 6.) c) and d) GIWAXS pattern of the film prepared with same condition as the films in a) and b), respectively.

transitions in hybrid organic–inorganic metal halide semiconductors, these criteria can only be satisfied in crystal systems with point symmetry that is monoclinic or lower (e.g., triclinic).^[53] In triclinic (R/S-MeOMePMA)BiI₄, symmetry analysis suggests that the exciton fine structure levels are in general non-degenerate and linearly polarized, but not mutually orthogonal (as would be the case, e.g., in an orthorhombic crystal, which should not exhibit apparent CD).

To further establish the strong correlation between the film orientation and the large g_{CD} from an apparent CD effect, we applied grazing-incidence wide-angle X-ray scattering (GIWAXS) to identify the preferred orientation (Figure 4c). For the film made from MeCN:DMSO = 9:1 (that shows the largest g_{CD} of ≈ 0.1), the (001) peak has a strong intensity in the out-of-plane direction but very weak in-plane signal. By contrast, the (010) peak shows strong in-plane signal but very weak out-of-plane signal, supporting a preferred orientation of the (001) plane parallel to the substrate. Moreover, the large g_{CD} values in these samples indicate that individual grains are predominantly aligned with their local reciprocal lattice vectors \mathbf{g}_{001} parallel to each other (since averaging between grains with antiparallel alignment would wash out the apparent CD effect).

We made additional modifications to the processing conditions to achieve thin films with a preferred (010) orientation by using only dimethyl sulfoxide (DMSO) as the processing sol-

vent and preheating the substrate to 65 °C. From the XRD pattern in Figure S7 (Supporting Information), the (001) peak in the DMSO-processed (S-MeOMePMA)BiI₄ film is much smaller than the films processed from DMF:DMSO = 4:1 at 65–70 °C, indicating the (010) plane parallel to the substrate is much preferred in films processed with DMSO only. We further carried out grazing incidence wide angle X-ray scattering (GIWAXS) to identify the preferred orientation of the film processed solely with dimethyl sulfoxide (DMSO), and the data (Figure 4d) indicates that the (001) peak only shows weak signal for both in-plane and out-of-plane directions while the (010) peak has a strong out-of-plane signal but very weak in-plane signal. These results support a strong preferred orientation of (010) plane parallel to the substrate in the DMSO-deposited thin films.

As shown in Figure 4b, the g_{CD} from the preferred (010)-oriented film was much smaller (≈ 0.003) than the preferred (001)-oriented film. The raw CD and absorption spectrum of DMSO processed (010) oriented film are shown in Figure S8 (Supporting Information), and the negligible CD response from racemic (MeOMePMA)BiI₄ film is also shown in Figure S8 (Supporting Information). Furthermore, there is almost no difference of g_{CD} values between the front and back measurements for this film. The calculated LDLB effect is almost zero, and averaged g_{CD} is almost the same as the front or back measured values, suggesting that the g_{CD} value obtained from this DMSO-processed

(010)-oriented film reflects the genuine CD without contribution from apparent CD. Importantly, the front-back averaged g_{CD} in the film with (010) preferred orientation is of the same order of magnitude (10^{-3}) to the averaged g_{CD} in the film with (001)-preferred orientation (despite some spectral differences, which we discuss below). The similar averaged g_{CD} magnitudes validate the practice of averaging g_{CD} from both measurements (front and back) to remove “apparent CD” effects and provide values more representative of the “genuine CD” of the material.

The data in Figure 4 indicate that thin films with a predominant (010) orientation parallel to the substrate do not display the “apparent CD” effect, in strong contrast to films with a predominant (001) orientation. Cross-polarized optical microscope images were taken to confirm the “apparent CD” effect in the (001) and (010) oriented films, as illustrated in Figure S9 (Supporting Information). In the case of the (001) oriented film, standard microscope images show the (001) film to be mostly illuminated and the overall shape in the images (Figure S9a,b, Supporting Information) remained mostly consistent. However, the major areas of the (001) oriented film displayed brightly and some small areas turned dark under crossed polarizers compared to without, suggesting the presence of local anisotropy in the film. This suggests a strong “apparent CD” effect in the largely anisotropic (001) oriented film. Conversely, the (010) oriented film demonstrated a different behavior. The image without crossed linear polarizers displayed a uniform gray background (Figure S9d, Supporting Information); but under crossed polarizers, most of the film turned black with very few areas appearing bright (Figure S9c, Supporting Information). This indicates that a significant portion of the film is without local anisotropy, leading to the conclusion that there is almost no “apparent CD” effect observed in the (010) oriented film.

To further investigate the distinctions between these orientations, we conducted surface scanning electron microscopy (SEM) analyses on both types of films to examine their morphologies. As revealed in Figure 5, films with a predominant (001) orientation exhibit large cracks but lack clearly identifiable grains. On the other hand, films with a predominant (010) orientation feature minute, randomly distributed grains embedded within the larger film matrix. This observed morphological contrast may contribute to the different CD effects observed in films with (001) and (010) orientations. Specifically, the random distribution of minute grains in the (010) oriented films could result in a diverse set of local g_{010} reciprocal lattice vectors. This dispersity may then lead to an averaging out of the apparent CD effect, particularly if the local g_{010} reciprocal lattice vectors of the grains have directions that are either parallel or antiparallel to the film normal.

Alternatively, the difference in the observed g_{CD} values from the two films processed with different solvents in our study could reflect a fundamental characteristic of the electronic structure of the (S-MeOMePMA)Bi₄. For example, Salij et al.^[40] showed that the apparent CD response is proportional to $\sin 2\theta$, where θ is the angle between two transition dipoles associated with non-degenerate transitions, which have significant components orthogonal to the direction of light propagation. Suppose the transition dipoles of the exciton fine structure levels are oriented along the primitive lattice vectors, then the ratio of the dissymmetry, g_{CD} , expected for the (010) and (001) films would be expected to scale as $g_{CD}^{(010)}/g_{CD}^{(001)} = \sin 2\beta/\sin 2\gamma = \approx 0.4$, all other factors be-

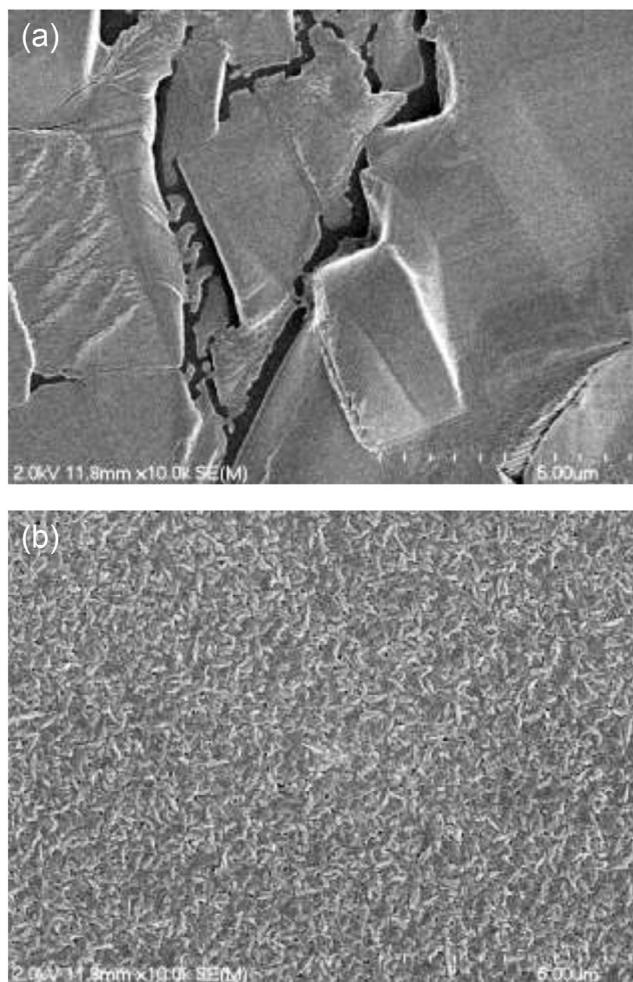


Figure 5. Surface SEM images for (a) (001) oriented films casted from MeCN:DMSO=9:1, preheated at 80 °C and (b) (010) oriented films casted from DMSO, preheated at 65 °C.

ing equal. The degree of dissymmetry also correlates directly with the energy separation between the involved transitions. If the a- and c-aligned transitions are more closely spaced energetically than the a- and the b-aligned transitions, these effects together could explain the much smaller apparent CD effect observed for the (010) oriented films relative to the (001) oriented films. Discriminating between the contributions of each of these potential effects will be the subject of future investigation.

Finally, we consider the observation that the genuine g_{CD} exhibits noticeable differences in spectral shape between films with preferred (001) and (010) orientations, as depicted in Figure 6. These differences persist even after averaging measurements from both the front and back sides of the films, and from four distinct positions during rotational measurements. Two potential mechanisms—or possibly a combination of both—could explain these observed differences. First, the CD signal itself may inherently differ depending on the crystal orientation.^[54] Different orientations could lead to variations in electronic structure and spin-orbital coupling, and thereby influence the absorption of circularly polarized light differently. Second, the distinct

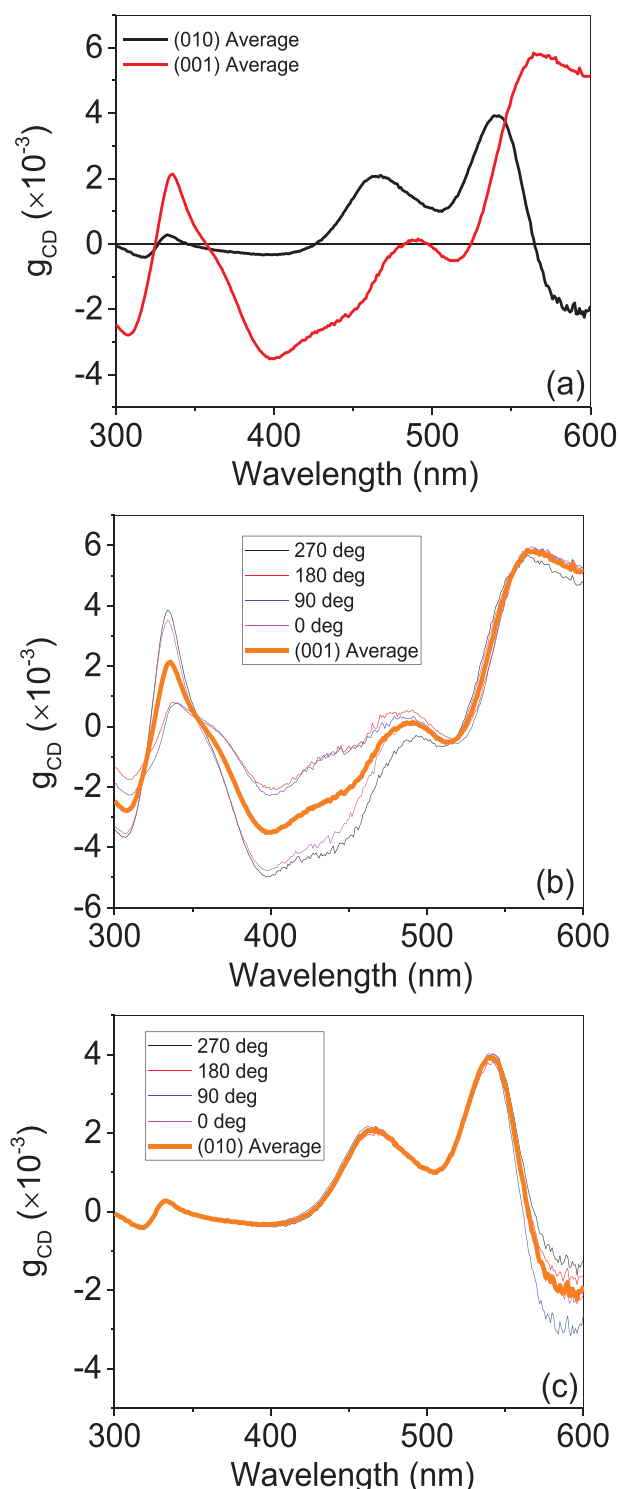


Figure 6. (a) genuine g_{CD} of (001) and (010) oriented films after taken the average of 4 different positions, plot of rotation measurement of averaged of front and back g_{CD} measured at 4 different positions, (0° , 90° , 180° , and 270°), (b) and (c) plot the g_{CD} (genuine) (i.e. average of front and back g_{CD}) as a function of four different rotational angles of the film (rotational angle defined within the x-y plane of the thin film) for (b) (001) predominant oriented film and (c) (010) predominant oriented film. The orange line in each panel represents the average of the four different rotational angles in each measurement.

morphologies of the films, as revealed by SEM (Figure 5), could result in differing light scattering behaviors, thereby affecting the measured g_{CD} . Therefore, the differences in genuine g_{CD} between the (001) and (010) oriented films could thus be attributed to either an inherent variation in CD signal due to crystal orientation, to differences in light scattering owing to diverse film morphologies, or to a combination of both factors. Altogether, these results support that the apparent CD effect in the 0D Bi-based hybrid organic-inorganic thin films exhibits a strong dependence on the preferred thin film orientation and morphology, which could be tuned by processing conditions. Since the “apparent CD” (LDLB) effect is a true light matter interaction, it holds great potential for augmenting the chiroptical response in OIHS based devices. This effect can offer significant benefits for applications such as CPL detection and emission. For example, the enhanced CD response and anisotropy factor from the “apparent CD” (LDLB) effect would further contribute to the overall photocurrent response or emission response for CPL detection and emission in OIHS based devices, in addition to the effect from the genuine CD.

3. Conclusion

In summary, the newly synthesized 0D Bi-based organic/inorganic metal halide hybrid, (*R/S*-MeOMePMA)Bi₄, shows strong chiroptical response, with g_{CD} values approaching 0.1. Through manipulation of deposition conditions and CD measurement conditions, we conclusively demonstrate that the major contribution of this unusually large g_{CD} is from the “apparent CD” effect. The observed large g_{CD} emerges when the thin film of our Bi-based hybrid organic-inorganic semiconductor adopts a preferred (001) orientation parallel to the substrate. Furthermore, the “apparent CD” effect was also found to depend strongly on the film orientation and morphology. When the film adopts preferred (010) orientation parallel to the substrate, the “apparent CD” effect was almost washed out due to the special morphology of the film, whereas films having well-crystallized preferred (001) orientation show strong “apparent CD” effect with a maximum value of the g_{CD} . Since the processing conditions of these Bi-based hybrids can be selected to favor one particular preferred orientation ((001) or (010)), our study provides a strategy for rational tuning of the chiroptical response and “apparent CD” effect of a self-assembled hybrid system. Taken together with other recent reports, it becomes clear that the large apparent CD effect, observed now across multiple material classes, is likely due to the low symmetry of such materials. Importantly, such large circular light-matter interaction can be further utilized for applications, such as circular polarized light detection and emission.

4. Experimental Section

Synthesis of *R/S*-MeOMePMAI: *R/S* MeOMePMAI was synthesized from the reaction of 2 mL of (*R*)-(+)-4-methoxy- α -methylbenzylamine or (*S*)-(–)-4-methoxy- α -methylbenzylamine (*R/S* 4-MeOMePMA, Sigma-Aldrich) with hydriodic acid (HI) (57 wt.% in water) with molar ratio 1:1.05 in 10 mL ethanol at 0°C for 1 h. The crude product was obtained by slowly evaporating the solvent under reduced pressure. Then the white

precipitate was dissolved and recrystallized in chloroform and washed with diethyl ether for three times. After drying overnight in vacuum oven at 50 °C, the product was transferred into a glove box filled with nitrogen for further use.

Synthesis of Single Crystal of (S-MeOMePMA)Bi₄: 41.9 mg of S-MeOMePMAI and 88.5 mg BiI₃ (Sigma–Aldrich) were dissolved in 1 mL acetonitrile, and the solution was filtered using a 0.2 μm PTFE filter. Then the solution was kept in a 4 mL vial, which was sealed by Teflon tape with a small hole. The 4 mL vial was put in a 20 mL vial with ≈10 mL dichloromethane. The dichloromethane slowly diffused into the 4 mL vial. After ≈1 week, red plate-like crystals were obtained.

Preparation of Thin Film of (R/S-MeOMePMA)Bi₄: R/S-MeOMePMAI and BiI₃ was dissolved in DMF:DMSO = 4:1 with 1:1 molar ratio at 0.3 M (Bi³⁺) concentration. The solution was filtered by 0.2 μm PTFE filter. Then the solution was spin coated on glass substrates (precleaned by sonicated in DI water, acetone, and isopropanol 15 min each) at 6000 rpm for 30 s and annealed at the targeted temperature (from 60 to 85 °C) for 10 min. For films prepared from DMSO, the concentration of Bi³⁺ is 0.3 M. The substrates were preheated at 65 °C for 5 min, and the solution was spun cast at 5000 rpm for 20 s, and the solution was annealing at 65 °C for 10 min. For films prepared from MeCN:DMSO = 9:1, the concentration of Bi³⁺ is 0.25 M. These substrates were preheated at 80 °C for 5 min, and the solution was spun cast at 5000 rpm for 20 s, followed by annealing at 80 °C for 10 min.

Single Crystal XRD: Single-crystal X-ray diffraction (SC-XRD) characterization for (S-MeOMePMA)Bi₄ was performed on a Rigaku XtaLAB Synergy-S diffractometer using Mo Kα radiation (λ = 0.71073 Å) and operating at 50 kV and 30 mA at room temperature (299 K) and 80 K. An 800 Series Cryostream Cooler was employed for the 80 K structure characterization. CrysAlisPro was used to perform peak hunting, data reduction, and numerical absorption correction for the collected data. The crystal structures were solved and refined using SHELXS direct methods and SHELXL least-squares method within the Olex2 software package. Symmetry analysis for the structure was performed using PLATON's ADDSYM-EXT tool with default positional/angular tolerance criteria, i.e., 0.3° angular tolerance factor for metric symmetry and 0.25 Å distance criterion for coinciding atoms for rotation, inversion, and translation symmetry elements.

Other General Measurement: Powder X-ray diffraction (XRD) and grazing-incidence wide-angle X-ray scattering (GIWAXS) were performed on a Rigaku SmartLab X-ray diffractometer using Cu Kα with 1D or 2D HyPix detector in parallel beam mode, respectively. The incidence angle was 0.2° and detector distance is ≈65.5 mm for GIWAXS measurement. The circular dichroism (CD) measurement was performed with a Chirascan V100 Spectropolarimeter (Applied Photophysics). All the plot images for crystal structures were drawn with VESTA 3 software.^[55]

Supporting Information

Supporting Information is available from the Wiley Online Library or from the author.

Acknowledgements

This work was primarily supported through the Center for Hybrid Organic Inorganic Semiconductors for Energy (CHOISE), an Energy Frontier Research Center funded by the U.S. Department of Energy (DOE), Office of Science, Office of Basic Energy Sciences (BES). The XRD, SEM and GIWAXS of perovskite thin films in this work was performed at the Chapel Hill Analytical and Nanofabrication Laboratory (CHANL), a member of the North Carolina Research Triangle Nanotechnology Network (RTNN), which is supported by the National Science Foundation, Grant ECCS-1542015 and ECCS-2025064, as part of the National Nanotechnology Coordinated Infrastructure, NNCI. The authors thank Josh Chen and Carrie Donley at CHANL for the assistance for GIWAXS measurement. The authors thank Amar S. Kumbhar at CHANL for the assistance for taking the SEM images. The authors thank Maruti Hegde and Prof. Theo Dingemans

in Department of Applied Physical Sciences at UNC Chapel Hill for the assistance for taking polarized microscope images. The CD measurement was performed at UNC Macromolecular Interactions Facility supported by the National Cancer Institute of the National Institutes of Health under award number P30CA016086. This work was authored, in part, by the National Renewable Energy Laboratory, operated by the Alliance for Sustainable Energy, LLC, for the US Department of Energy (DOE) under contract no. DE-AC36-08GO28308. The views expressed in the article do not necessarily represent the views of the DOE or the US government.

Correction added on February 12, 2024: Correction in Supporting information.

Conflict of Interest

The authors declare no conflict of interest.

Data Availability Statement

The data that support the findings of this study are available in the supplementary material of this article.

Keywords

chiroptic response, hybrid organic–inorganic metal halide, preferred orientation

Received: November 1, 2023

Revised: January 4, 2024

Published online:

- [1] D. B. Mitzi, K. Chondroudis, C. R. Kagan, *IBM J. Res. Dev.* **2001**, *45*, 29.
- [2] B. Saparov, D. B. Mitzi, *Chem. Rev.* **2016**, *116*, 4558.
- [3] L. Mao, C. C. Stoumpos, M. G. Kanatzidis, *J. Am. Chem. Soc.* **2019**, *141*, 1171.
- [4] M. D. Smith, B. A. Connor, H. I. Karunadasa, *Chem. Rev.* **2019**, *119*, 3104.
- [5] J. Hu, L. Yan, W. You, *Adv. Mater.* **2018**, *30*, 1802041.
- [6] H. Yang, S. Mandal, Y. H. Lee, J. Y. Park, H. Zhao, C. Yuan, L. Huang, M. Chen, L. Dou, *J. Am. Chem. Soc.* **2023**, *145*, 23963.
- [7] W. Paritmongkol, W. S. Lee, W. Shcherbakov-Wu, S. K. Ha, T. Sakurada, S. J. Oh, W. A. Tisdale, *ACS Nano* **2022**, *16*, 2054.
- [8] L. Maserati, S. Refaely-Abramson, C. Kastl, C. T. Chen, N. J. Borys, C. N. Eisler, M. S. Collins, T. E. Smidt, E. S. Barnard, M. Strasbourg, E. A. Schriber, B. Shevitski, K. Yao, J. N. Hohman, P. J. Schuck, S. Aloni, J. B. Neaton, A. M. Schwartzberg, *Mater. Horiz.* **2021**, *8*, 197.
- [9] Y. Dang, X. Liu, B. Cao, X. Tao, *Matter* **2021**, *4*, 794.
- [10] G. Long, R. Sabatini, M. I. Saidaminov, G. Lakhwani, A. Rasmita, X. Liu, E. H. Sargent, W. Gao, *Nat. Rev. Mater.* **2020**, *5*, 423.
- [11] Y. Dong, Y. Zhang, X. Li, Y. Feng, H. Zhang, J. Xu, *Small* **2019**, *15*, 1902237.
- [12] L. Guo, S. Hu, X. Gu, R. Zhang, K. Wang, W. Yan, X. Sun, *Adv. Mater.* **2023**, 2301854, <https://doi.org/10.1002/adma.202301854>.
- [13] M. W. Heindl, T. Kodalle, N. Fehn, L. K. Reb, S. Liu, C. Harder, M. Abdelsamie, L. Eyre, I. D. Sharp, S. V. Roth, P. Müller-Buschbaum, A. Kartouzian, C. M. Sutter-Fella, F. Deschler, *Adv. Opt. Mater.* **2022**, *10*, 2200204.
- [14] J. Ahn, E. Lee, J. Tan, W. Yang, B. Kim, J. Moon, *Mater. Horiz.* **2017**, *4*, 851.
- [15] L. Yan, M. K. Jana, P. C. Sercel, D. B. Mitzi, W. You, *J. Am. Chem. Soc.* **2021**, *143*, 18114.

- [16] Z. Wang, C.-C. Lin, K. Murata, A. S. A. Kamal, B.-W. Lin, M.-H. Chen, S. Tang, Y.-L. Ho, C.-C. Chen, C.-W. Chen, H. Daiguji, K. Ishii, J.-J. Delaunay, *Adv. Mater.* **2023**, *35*, 2303203.
- [17] S. Liu, M. Kepenekian, S. Bodnar, S. Feldmann, M. W. Heindl, N. Fehn, J. Zerhoch, A. Shcherbakov, A. Pöthig, Y. Li, U. W. Paetzold, A. Kartouzian, I. D. Sharp, C. Katan, J. Even, F. Deschler, *Sci. Adv.* **2023**, *9*, eadh5083.
- [18] J. Ma, C. Fang, C. Chen, L. Jin, J. Wang, S. Wang, J. Tang, D. Li, *ACS Nano* **2019**, *13*, 3659.
- [19] Y. Zhou, Y. Huang, X. Xu, Z. Fan, J. B. Khurgin, Q. Xiong, *Appl. Phys. Rev.* **2020**, *7*, 041313.
- [20] Y. Zheng, J. Xu, X.-H. Bu, *Adv. Opt. Mater.* **2022**, *10*, 2101545.
- [21] C. Yuan, X. Li, S. Semin, Y. Feng, T. Rasing, J. Xu, *Nano Lett.* **2018**, *18*, 5411.
- [22] L. Zhao, X. Han, Y. Zheng, M.-H. Yu, J. Xu, *Adv. Photon. Res.* **2021**, *2*, 2100056.
- [23] D. H. Waldeck, R. Naaman, Y. Paltiel, *APL Mater.* **2021**, *9*, 040902.
- [24] J. Wang, B. Mao, Z. V. Vardeny, *J. Chem. Phys.* **2023**, *159*, 091002.
- [25] Q. Wang, H. Zhu, Y. Tan, J. Hao, T. Ye, H. Tang, Z. Wang, J. Ma, J. Sun, T. Zhang, F. Zheng, W. Zhang, H. W. Choi, W. C. H. Choy, D. Wu, X. W. Sun, K. Wang, *Adv. Mater.* **2023**, 2305604, <https://doi.org/10.1002/adma.202305604>.
- [26] K. Kim, E. Vetter, L. Yan, C. Yang, Z. Wang, R. Sun, Y. Yang, A. H. Comstock, X. Li, J. Zhou, L. Zhang, W. You, D. Sun, J. Liu, *Nat. Mater.* **2023**, *22*, 322.
- [27] A. Ishii, T. Miyasaka, *Sci. Adv.* **2020**, *6*, eabd3274.
- [28] B. Nordén, A. Rodger, T. Dafforn, *Linear Dichroism and Circular Dichroism*, Royal Society of Chemistry, London, **2010**.
- [29] S. Liu, M. W. Heindl, N. Fehn, S. Caicedo-Dávila, L. Eyre, S. M. Kronawitter, J. Zerhoch, S. Bodnar, A. Shcherbakov, A. Stadlbauer, G. Kieslich, I. D. Sharp, D. A. Egger, A. Kartouzian, F. Deschler, *J. Am. Chem. Soc.* **2022**, *144*, 14079.
- [30] S. Jiang, P. Zhao, G. Xing, H. Kang, X. Li, T. Zhao, B. Li, T. Zhang, *Adv. Opt. Mater.* **2023**, *11*, 2203078.
- [31] J. Hao, H. Lu, L. Mao, X. Chen, M. C. Beard, J. L. Blackburn, *ACS Nano* **2021**, *15*, 7608.
- [32] J. Ma, H. Wang, D. Li, *Adv. Mater.* **2021**, *33*, 2008785.
- [33] G. Albano, G. Pescitelli, L. Di Bari, *Chem. Rev.* **2020**, *120*, 10145.
- [34] G. Albano, M. Lissia, G. Pescitelli, L. A. Aronica, L. Di Bari, *Mater. Chem. Front.* **2017**, *1*, 2047.
- [35] G. Albano, F. Salerno, L. Portus, W. Porzio, L. A. Aronica, L. Di Bari, *ChemNanoMat* **2018**, *4*, 1059.
- [36] G. Albano, M. Górecki, G. Pescitelli, L. Di Bari, T. Jávorfí, R. Hussain, G. Siligardi, *New J. Chem.* **2019**, *43*, 14584.
- [37] F. Zinna, G. Albano, A. Taddeucci, T. Colli, L. A. Aronica, G. Pescitelli, L. Di Bari, *Adv. Mater.* **2020**, *32*, 2002575.
- [38] Z. Zhang, Z. Wang, H. H.-Y. Sung, I. D. Williams, Z.-G. Yu, H. Lu, *J. Am. Chem. Soc.* **2022**, *144*, 22242.
- [39] G. Albano, G. Pescitelli, L. Di Bari, *ChemNanoMat* **2022**, *8*, 202200219.
- [40] A. Salij, R. H. Goldsmith, R. Tempelaar, *J. Am. Chem. Soc.* **2021**, *143*, 21519.
- [41] S. Ma, Y.-K. Jung, J. Ahn, J. Kyhm, J. Tan, H. Lee, G. Jang, C. U. Lee, A. Walsh, J. Moon, *Nat. Commun.* **2022**, *13*, 3259.
- [42] C. Chen, L. Gao, W. Gao, C. Ge, X. Du, Z. Li, Y. Yang, G. Niu, J. Tang, *Nat. Commun.* **2019**, *10*, 1927.
- [43] Y.-H. Kim, Y. Zhai, H. Lu, X. Pan, C. Xiao, E. A. Gauding, S. P. Harvey, J. J. Berry, Z. V. Vardeny, J. M. Luther, M. C. Beard, *Science* **2021**, *371*, 1129.
- [44] T. J. Ugras, Y. Yao, R. D. Robinson, *Chirality* **2023**, *35*, 846.
- [45] N. Kobayashi, A. Muranaka, *Circular Dichroism and Magnetic Circular Dichroism Spectroscopy for Organic Chemists*, The Royal Society of Chemistry, London, **2012**.
- [46] J. Yeom, U. S. Santos, M. Chekini, M. Cha, A. F. De Moura, N. A. Kotov, *Science* **2018**, *359*, 309.
- [47] A. O. El-Ballouli, O. M. Bakr, O. F. Mohammed, *J. Phys. Chem. Lett.* **2020**, *11*, 5705.
- [48] Y. Xu, M. Wang, Y. Lei, Z. Ci, Z. Jin, *Adv. Energy Mater.* **2020**, *10*, 2002558.
- [49] J. C. Hamill, J. Schwartz, Y.-L. Loo, *ACS Energy Lett.* **2018**, *3*, 92.
- [50] D. N. Dirin, S. Dreyfuss, M. I. Bodnarchuk, G. Nedelcu, P. Papagiorgis, G. Itkos, M. V. Kovalenko, *J. Am. Chem. Soc.* **2014**, *136*, 6550.
- [51] J. Sanderson, C. A. Bayse, *Tetrahedron* **2008**, *64*, 7685.
- [52] J. Dong, S. Shao, S. Kahmann, A. J. Rommens, D. Hermida-Merino, G. H. Ten Brink, M. A. Loi, G. Portale, *Adv. Funct. Mater.* **2020**, *30*, 2001294.
- [53] G. F. Koster, J. O. Dimmock, R. G. Wheeler, *Properties of the Thirty-Two Point Groups*, M.I.T. Press, Cambridge **1963**.
- [54] Y. Bing, D. Selassie, R. H. Paradise, C. Isborn, N. Kramer, M. Sadilek, W. Kaminsky, B. Kahr, *J. Am. Chem. Soc.* **2010**, *132*, 7454.
- [55] K. Momma, F. Izumi, *J. Appl. Crystallogr.* **2011**, *44*, 1272.